Localized solutions in parametrically driven pattern formation

Tae-Chang Jo and Dieter Armbruster*
Department of Mathematics, Arizona State University, Tempe, Arizona 85287-1804, USA
(Received 28 October 2002; published 16 July 2003)

The Mathieu partial differential equation (PDE) is analyzed as a prototypical model for pattern formation due to parametric resonance. After averaging and scaling, it is shown to be a perturbed nonlinear Schrödinger equation (NLS). Adiabatic perturbation theory for solitons is applied to determine which solitons of the NLS survive the perturbation due to damping and parametric forcing. Numerical simulations compare the perturbation results to the dynamics of the Mathieu PDE. Stable and weakly unstable soliton solutions are identified. They are shown to be closely related to oscillons found in parametrically driven sand experiments.

DOI: 10.1103/PhysRevE.68.016213 PACS number(s): 89.75.−k

I. INTRODUCTION

The standard model for the instability of a harmonic oscillator due to parametric forcing (parametric resonance) is the Mathieu equation [1] which can be written as

$$A_{tt}+(\omega^2+\epsilon\cos qt)A=0. \tag{1}$$

Here, ω is the eigenfrequency of the oscillator, ϵ is a small forcing amplitude, and q is the forcing frequency. The trivial equilibrium becomes unstable if $\omega/q=k/2$, $k=1,2,\ldots$. By including nonlinearity and damping, the Mathieu equation has become a prototype nonlinear oscillator for studying parametric resonance, in much the same way as the Lorenz system and the van der Pol oscillator represent chaos and self-excited oscillations, respectively [2].

Recently, Rand *et al.* [3,4] and Armbruster *et al.* [5] have included spatial interactions into the Mathieu equation to study the continuum limit of a line of coupled pendula with vertical forcing [3] and to describe the pattern formation due to the parametrically driven forcing. Motivating physical experiments for the pattern formation aspects include the Faraday experiment of a vibrating layer of fluid [6] and related experiments on vertically vibrating layers of sand [7]. In all cases, the trivial equilibrium becomes unstable at a particular forcing frequency and forcing amplitude, creating patterns of surface waves (sand patterns) that oscillate with half the frequency of the forcing. It is hoped [5] that the spatially extended Mathieu equation [the Mathieu partial differential equation (PDE)] can be considered as a prototype for these parametrically forced pattern formations, in such a way that certain features in parametrically forced pattern formation experiments are universal, i.e., independent of the specific physical mechanisms. The resonance region (Arnold tongue [1]) for the 2:1 resonance ($k=1$) is the largest in parameter space, while higher-order Arnold tongues quickly close up. We therefore concentrate the following discussion on the 2:1 resonance.

In addition to regular patterns, very localized patterns have been observed in these experiments. Standing solitary waves were observed in Faraday experiments with fluids in Ref. [8]. The most spectacular localized phenomena are called oscillons [9]. An oscillon is a small, circularly symmetric time dependent excitation that resembles an active volcano. It is subharmonic, that is, the frequency of the oscillon is half of the driving frequency. The oscillon resembles a peak during one cycle of the container and a crater on the next cycle. The experiments show hysteresis: An oscillon can be observed only when the forcing amplitude decreases in a certain range of the forcing frequency.

Localized structures have been discussed for various models: the nonlinear Schrödinger equation [10,11], the Ginzburg Landau equation [12–17], the Swift Hohenberg equation [18], and others. Localized structures are, in general, explained through a homoclinic or heteroclinic orbit (solitons) in a dynamical system [19,20]. Previous work on the study of localized pattern formation related to parametric resonance includes specific hydrodynamic models for the analysis of the Faraday experiments [21]. The resulting cubic nonlinear Schrödinger equation was analyzed by Laedke and Spatschek [22] and by Elphick and Meron [23].

The Mathieu PDE has been studied using a low-dimensional Galerkin approximation in Refs. [3,4]. It shows pattern formation through one or a few spatial modes. However, since any localized structure has a very broad Fourier spectrum, a low-dimensional Galerkin approximation necessarily misses localized structures. The Mathieu PDE has also been studied using averaging [5]. The averaged Mathieu equation turns out to be similar to the complex Ginzburg Landau equation or the nonlinear Schrödinger equation (NLS). Armbruster *et al.* [5] performed local bifurcation analysis and a numerical path following analysis, which are restricted to a small number of Fourier modes. They were therefore not able to study localized structures.

This study takes advantage of the fact that the averaged Mathieu PDE can be considered as a perturbation of the nonlinear Schrödinger equation. Specifically, the NLS is integrable and has a continuum of soliton solutions, which are spatially localized standing or traveling waves. Using adiabatic perturbation theory for solitons developed in Ref. [24], we derive a set of ordinary differential equations (ODEs) that describe the behavior of the soliton solutions under perturbations. We show that these ODEs have nontrivial steady state solutions, which represent solitons that survive the perturbations and that resemble spatially localized solutions of the NLS. Numerical simulations of the NLS and of the Mathieu PDE confirm the existence of these steady and oscillating

*Electronic address: armbruster@asu.edu

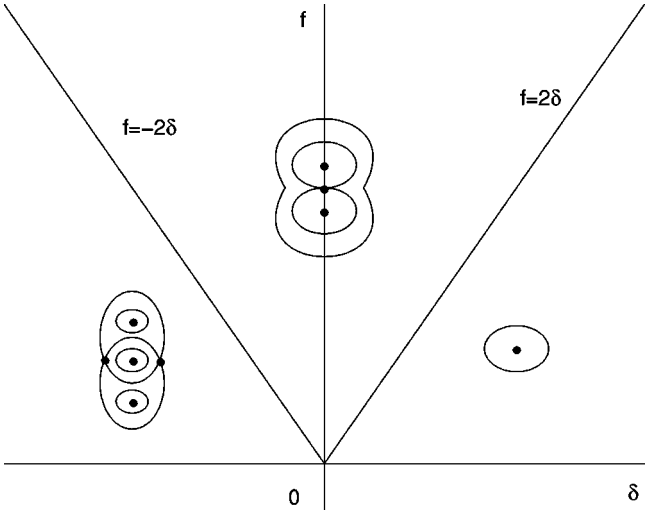

FIG. 1. Phase portraits for the undamped nonlinear Mathieu equation (ODE) for $\alpha<0$ in Eq. (2).

solitons, respectively. Depending on the perturbation parameters, the stable steady state of the ODEs corresponds to stable or weakly unstable solutions of the PDEs.

The rest of this paper is organized as follows. Section II starts out from the averaged Mathieu PDE. It is shown to be a specific perturbation of the NLS. Section II B uses the adiabatic approximation to the NLS to derive a set of ODEs. Section II C analyzes these equations, and Sec. III compares the numerical simulations of the ODE, the NLS, and the Mathieu PDE near the localized solutions. We conclude by discussing the relationship of our work to Ref. [22] and with an outlook for further work.

II. THE MATHIEU PDE

We consider a 2:1 resonance case for our study of Eq. (1) and add weak detuning, damping, spatial coupling, and a cubic nonlinearity. The resulting system, called the Mathieu partial differential equation, is

$$A_{tt}+A=\epsilon(\delta A-\gamma A_t-\alpha A^3+f\cos 2tA+dA_{xx}), \qquad (2)$$

where A is a scalar variable and δ,γ,f,d,α are constants for detuning, damping, parametric forcing, spatial coupling, and nonlinearity, respectively.

The ordinary differential equation for the case of $d=0$ has been discussed in many papers (e.g., Refs. [25–27]). Phase portraits for an undamped Mathieu equation are shown in Fig. 1. In the case of negative α, the zero solution bifurcates subcritically at the bifurcation parameter $f=0$ when δ is negative, and bifurcates supercritically at $f=2\delta$ when δ is positive. For $0<f<-2\delta$ and $\delta<0$, the system is bistable.

Following the analysis in Ref. [5], we can average Eq. (2) to get

$$u_t=\frac{\epsilon}{2}\left[i\left\{\delta u+du_{xx}-\frac{3\alpha}{4}|u|^2u+\frac{f}{2}\overline{u}\right\}-\gamma u\right]. \qquad (3)$$

At this stage, the averaging procedure is purely formal. However, assuming that attractors of the Mathieu PDE (2) and the averaged Eq. (3) can be captured by finite-dimensional systems, the averaging theorem for ODEs applies and hence solutions to the averaged equation stay $O(\epsilon)$ close to the solutions of the original equation on a time scale of $O(1/\epsilon)$ [26].

Under the assumption that forcing, damping and, detuning (the parameters f,γ, and δ) are one order of magnitude smaller than spatial coupling and nonlinearity (d and α), we can transform the averaged Mathieu PDE (3). The transformations

$$t'=\left(\frac{\epsilon}{2}\right)t, \quad x'=\left(\frac{1}{\sqrt{2d}}\right)x, \quad u'=\left(\sqrt{-\frac{3\alpha}{4}}\right)u \qquad (4)$$

lead to the scaled averaged Mathieu PDE

$$iu_t+\frac{1}{2}u_{xx}+|u|^2u=-\delta u-i\gamma u-\frac{f}{2}\overline{u}, \qquad (5)$$

where we have dropped the prime after the transformations. After another transformation

$$u'=\exp(-i\delta t)u, \qquad (6)$$

we can write Eq. (5) as a perturbed standard nonlinear Schrödinger equation

$$iu_t+\frac{1}{2}u_{xx}+|u|^2u=\epsilon P, \qquad (7)$$

where

$$\epsilon P=-i\gamma u-\frac{f}{2}\overline{u}\exp(-2i\delta t) \qquad (8)$$

is a small perturbation that slowly oscillates in time. From now on, we assume $\alpha<0$ which corresponds to a NLS with focusing cubic nonlinearity. The parameters γ, δ, and f are assumed to be $O(\epsilon)$ in Eq. (8). We also assume that the domain of the x variable is $(-\infty,\infty)$ and that the equation has fast decaying zero boundary conditions at $x=\pm\infty$. The following section will study Eq. (7) in detail. While there exist many studies that analyzed the damped and driven NLS ([28,29,22,30]), they all focused on direct forcing, leading to an extra constant term. They did not consider parametric forcing [represented in P by the term involving $\overline{u}$ in Eq. (8)]. The only other analysis that deals with parametric forcing is Ref. [22]. We will comment on their work in the Conclusion.

A. The perturbed nonlinear Schrödinger equation

A single soliton solution to the nonlinear Schrödinger [Eq. (7) with $\epsilon=0$] can be written as

$$u(x,t)=2\nu\,\mathrm{sech}[2\nu(x-2\mu t-x_0)]\exp[i2\mu(x-2\mu t-x_0)+i(2\mu^2+2\nu^2)t+i\sigma_0], \qquad (9)$$

for constants ν, μ, x_0, and σ_0, as shown in Ref. [31]. The constant ν determines the amplitude and the pulse width of the solitary wave. Its speed and frequency are affected by the constant μ, and its phase constants are determined by the other two constants x_0 and σ_0. For the general type of solitary wave solutions (9), the amplitude of the pulse is inversely proportional to the pulse width. The speed of the solitary wave solution is independent of the pulse amplitude, which differs from the solitary wave solution of the Korteweg de Vries equation.

The nonlinear Schrödinger equation has been studied with different perturbations. Dissipative terms, some forcing terms, dispersion terms, some random functions as well as numerical simulation have been discussed in Refs. [31,32,24,10]. In general, if the perturbation is purely dissipative, it damps the soliton solution and eventually destroys the soliton. For general perturbations, a balance may exist which allows some solitons to survive.

B. Adiabatic approximation

To determine this balance, we are using the adiabatic perturbation theory [24] developed for the evolution of a single soliton solution under perturbations. Specifically, we parametrize amplitude, frequency, velocity, and phase of the soliton, and neglect any other changes in the shape of the pulse and tail formation.

Therefore, we look for the soliton pulse solution to the perturbed nonlinear Schrödinger equation (7) in the form of

$$u(x,t)=2\nu\,\mathrm{sech}\,\kappa\exp(i\mu\kappa/\nu+i\omega),\quad \kappa=2\nu(x-\xi). \tag{10}$$

The envelope of the approximation (the sech profile) is kept during the time evolution. In addition, we have some balance between the amplitude and the width of the pulse, that is, the inverse proportionality between them.

With this ansatz, the parameters in Eq. (10) evolve according to the following system of ordinary differential equations:

$$\frac{d\mu}{dt}=\frac{\epsilon}{2}\mathrm{Im}\int_{-\infty}^{\infty}\frac{\tanh\kappa}{\cosh\kappa}(-iP)e^{-i\mu\kappa/\nu-i\omega}d\kappa, \tag{11}$$

$$\frac{d\nu}{dt}=\frac{\epsilon}{2}\mathrm{Re}\int_{-\infty}^{\infty}\mathrm{sech}\,\kappa(-iP)e^{-i\mu\kappa/\nu-i\omega}d\kappa, \tag{12}$$

$$\frac{d\xi}{dt}=2\mu+\frac{\epsilon}{4\nu^2}\mathrm{Re}\int_{-\infty}^{\infty}\frac{\kappa}{\cosh\kappa}(-iP)e^{-i\mu\kappa/\nu-i\omega}d\kappa, \tag{13}$$

$$\frac{d\omega}{dt}=2\mu\frac{d\xi}{dt}-2\mu^2+2\nu^2+\frac{\epsilon}{2\nu}\mathrm{Im}\int_{-\infty}^{\infty}\frac{1-\kappa\tanh\kappa}{\cosh\kappa}\times(-iP)e^{-i\mu\kappa/\nu-i\omega}d\kappa, \tag{14}$$

where P stands for the perturbation [Eq. (8)] evaluated with the ansatz $u(x,t)$ of Eq. (10). For the case of pure dissipative perturbation ($\gamma>0$ and $f=0$), the integrals of the right-hand sides reduce to

$$\frac{d\mu}{dt}=0,\quad \frac{d\nu}{dt}=-2\gamma\nu, \tag{15}$$

$$\frac{d\xi}{dt}=2\mu,\quad \frac{d\omega}{dt}=2\mu^2+2\nu^2. \tag{16}$$

These equations can easily be solved to give

$$\mu=\mu_0,\quad \nu=\nu_0\exp(-2\gamma t), \tag{17}$$

$$\xi=2\mu_0 t+\xi_0,\quad \omega=-\frac{\nu_0^2}{2\gamma}[\exp(-4\gamma t)-1]+2\mu_0^2 t+\omega_0, \tag{18}$$

where μ_0, ν_0, ξ_0, and ω_0 are initial conditions for μ, $\nu\xi$, and ω, respectively. The amplitude of the solitary solution (2ν) decays with time for positive γ, as expected. If the initial speed ($2\mu_0$) of the soliton is nonzero, the soliton oscillates and drifts, but dies out.

C. The perturbation equations

Using complex integration, the integrals of Eqs. (11)–(14) can be evaluated (see the Appendix). The resulting system of ordinary differential equations is

$$\frac{d\mu}{dt}=-\frac{f\pi\mu^2}{\nu}\mathrm{csch}\left(\frac{\pi\mu}{\nu}\right)\sin(2\omega+2\delta t), \tag{19}$$

$$\frac{d\nu}{dt}=-2\gamma\nu+f\pi\mu\,\mathrm{csch}\left(\frac{\pi\mu}{\nu}\right)\sin(2\omega+2\delta t), \tag{20}$$

$$\frac{d\xi}{dt}=2\mu+\frac{f\pi}{4\nu}\mathrm{csch}\left(\frac{\pi\mu}{\nu}\right)\left[\frac{\pi\mu}{\nu}\coth\left(\frac{\pi\mu}{\nu}\right)-1\right]\cos(2\omega+2\delta t), \tag{21}$$

$$\frac{d\omega}{dt}=2\mu^2+2\nu^2+\frac{f\pi\mu}{2\nu}\mathrm{csch}\left(\frac{\pi\mu}{\nu}\right)\times\left[\frac{2\pi\mu}{\nu}\coth\left(\frac{\pi\mu}{\nu}\right)-1\right]\cos(2\omega+2\delta t). \tag{22}$$

Note that ξ decouples and we only have a system of three variables. We use new variables η and $\tilde{\omega}$ such that

$$\eta=\frac{\mu}{\nu},\quad \tilde{\omega}=\omega+\delta t \tag{23}$$

to get a system of three autonomous equations:

$$\frac{d\eta}{dt}=2\eta\left[\gamma-\frac{f\pi\eta}{\sinh(\pi\eta)}\sin(2\tilde{\omega})\right], \tag{24}$$

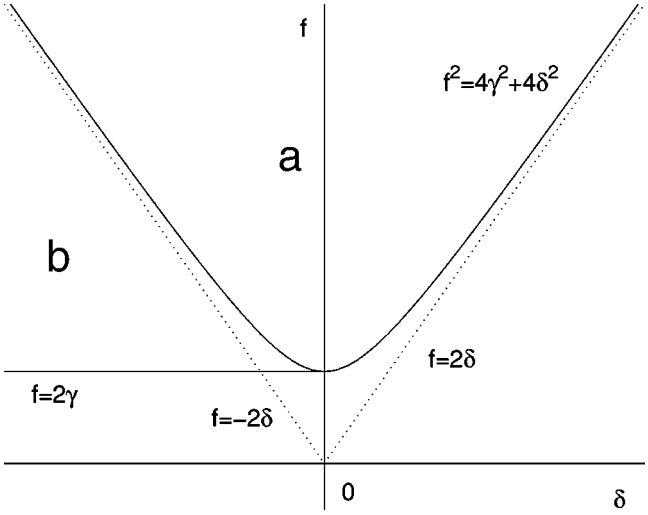

FIG. 2. Parameter regions for the existence of nontrivial fixed points of the ordinary differential equations (24)–(26): (*a*) One stable nontrivial fixed point. (*b*) Two nontrivial fixed points, one stable and one unstable.

$$\frac{d\nu}{dt}=\nu\left[-2\gamma+\frac{f\pi\eta}{\sinh(\pi\eta)}\sin(2\tilde{\omega})\right], \tag{25}$$

$$\frac{d\tilde{\omega}}{dt}=\delta+2\nu^2(\eta^2+1)+\frac{f\pi\eta}{2\sinh(\pi\eta)}\times\left[\frac{2\pi\eta\cosh(\pi\eta)}{\sinh(\pi\eta)}-1\right]\cos(2\tilde{\omega}). \tag{26}$$

The right-hand sides are not defined when $\eta=0$ since $\sinh(0)=0$, but the limit exists such that at $\eta=0$ we define

$$\frac{d\eta}{dt}=0,\quad \frac{d\nu}{dt}=\nu[-2\gamma+f\sin(2\tilde{\omega})],$$

$$\frac{d\tilde{\omega}}{dt}=\delta+2\nu^2+\frac{f}{2}\cos(2\tilde{\omega}). \tag{27}$$

The nontrivial fixed points ($\nu>0$) are

$$\eta_*=0,\quad \nu_*=\left(-\frac{1}{2}\delta\pm\frac{1}{4}\sqrt{f^2-4\gamma^2}\right)^{1/2},$$

$$\tilde{\omega}_*=\frac{1}{2}\arctan\left(-\frac{\gamma}{2\nu_*^2+\delta}\right). \tag{28}$$

There is only one nontrivial fixed point for $f>\sqrt{4\delta^2+4\gamma^2}$ [region *a* in Fig. 2]. There are two nontrivial fixed points for $2\gamma<f<\sqrt{4\delta^2+4\gamma^2}$ when $\delta<0$ [region *b* in Fig. 2]. Note that $d\xi/dt$ is also zero at the fixed point $(\eta_*,\nu_*,\tilde{\omega}_*)$, which gives us the constant solution $\xi=\xi_*$. These results raise an important issue on the order of magnitude of the detuning δ. While the original perturbation [Eq. (7)] places no restriction on the order of magnitude of δ, the above results for the fixed points clearly indicate that all the parameters f, γ, and δ have to be of the same order of magnitude. This implies that the adiabatic perturbation theory is an unfolding analysis in a full neighborhood of zero for those three parameters.

The eigenvalues of the linearized system at these fixed points are

$$\lambda=-2\gamma,-\gamma\pm\sqrt{\gamma^2+8f\nu_*^2\cos(2\tilde{\omega}_*)} \tag{29}$$

giving us a stable fixed point for $\cos(2\tilde{\omega}_*)<0$. Since $f>\sqrt{4\delta^2+4\gamma^2}$ in region *a*, the only nontrivial fixed point is stable. In region *b*, one fixed point is stable and the other is unstable (Fig. 2). The soliton

$$u(x,t)=2\nu_*\mathrm{sech}(2\nu_*(x-\xi_*))\exp(i\tilde{\omega}_*) \tag{30}$$

corresponding to a fixed point is the corresponding approximate solution to the perturbed nonlinear Schrödinger equation (5). It is a steady solution that neither drifts nor oscillates. It becomes an approximation of a solution to the averaged Mathieu equation (3) after recovering the time scale *t*, the length scale *x*, and the scale for the solution *u*.

Here,

$$A(x,t)=2\nu_*\mathrm{sech}(2\nu_*(x-\xi_*))\cos(t-\tilde{\omega}_*) \tag{31}$$

is the approximate solution to the Mathieu partial differential equation. It has a pulselike spatial structure and can be expected to be a good approximation on a time scale of the order of $1/\epsilon$. Note that the solution (31) does not drift but oscillates with a period of 2π, twice the forcing period.

III. NUMERICAL SIMULATIONS

To study the validity of our multistage perturbation analysis, we simulate three different equations and compare them. First, we simulate the three-dimensional (3D) ordinary differential equations (24)–(26). Second, we simulate the scaled averaged Mathieu PDE (the perturbed NLS) (5). We use a central difference scheme for space differentiation and a Crank-Nicolson method for time integration. Last, we simulate the time dependent Mathieu PDE (2). We use central difference schemes for both space and time differentiations. The goal of these simulations is to determine whether attraction to the stable nontrivial equilibria found analytically in the ODEs (24)–(26) corresponds to attraction to stable solitons in the perturbed NLS and to stable localized oscillonlike solutions in the Mathieu PDE.

A. Ordinary differential equations

We simulate the system of ordinary differential equations (24)–(26) with the parametrs $f=0.05$, $\delta=0.01$, and $\gamma=0.0125$. Figures 3(a)–3(c) shows the time evolutions of each variable with various initial conditions. Solutions approach the nontrivial fixed point. Note that the variable $|\eta|$ always decreases and variables (μ,ω) spiral in after some transient time as the linear stability analysis suggested.

The simulations also confirm the numerical value of the nontrivial fixed point. The nontrivial fixed point, however, is

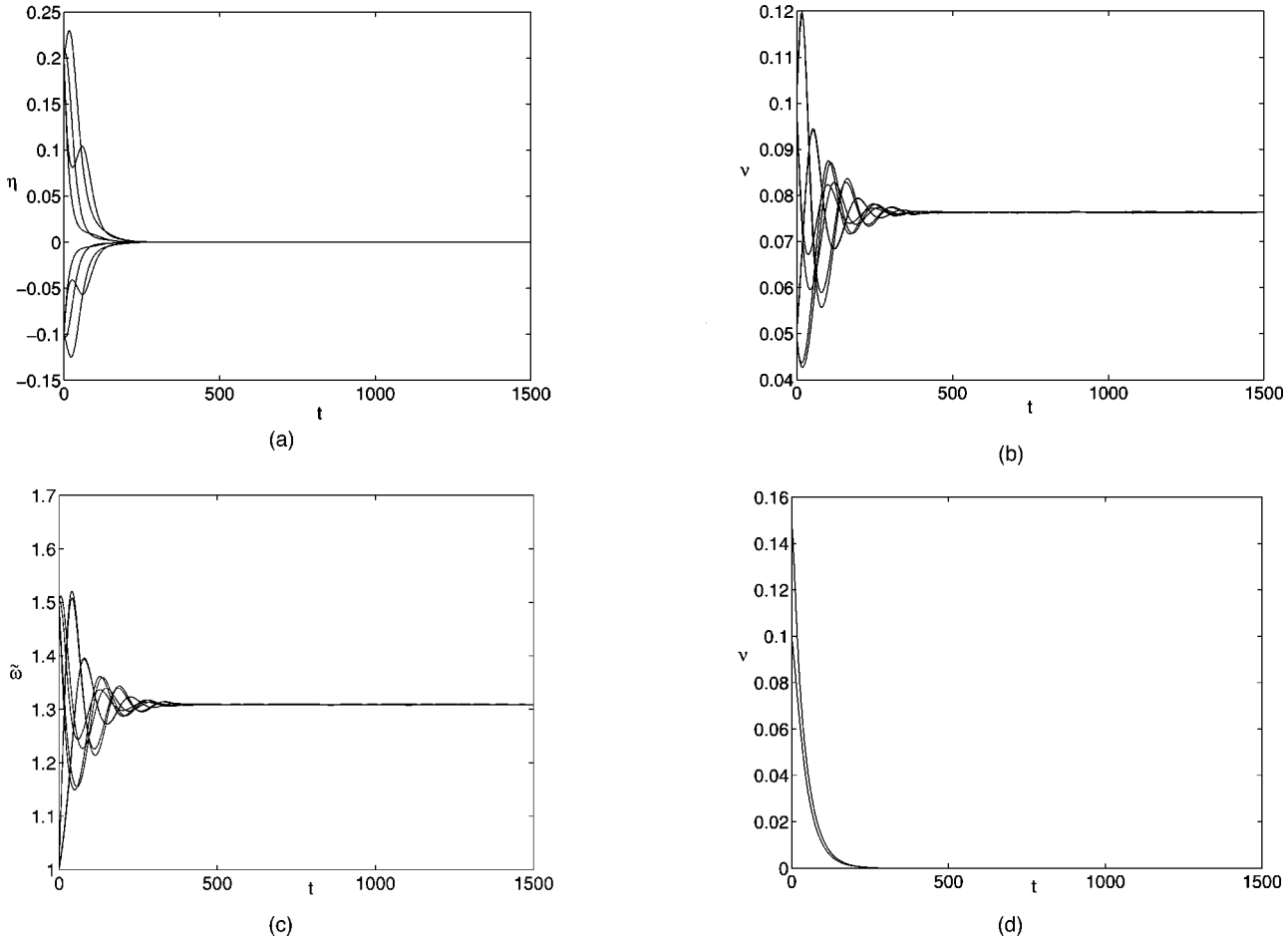

FIG. 3. Time evolution of solutions to Eqs. (24)–(26) for $f=0.05$, $\delta=0.01$, and $\gamma=0.0125$, and various initial conditions: (a) η, (b) ν, (c) $\tilde{\omega}$, and (d) ν.

not a global attractor. The solutions approach zero for some initial conditions as shown in Fig. 3(d). The basin of attraction for the nontrivial fixed point is mainly constrained by η being small enough.

The time evolution of the corresponding adiabatically approximated soliton is shown in Fig. 4 at time $t=0$, 25, and 1500. The profile at $t=1500$ in Fig. 4 is almost the same as the nontrivial fixed point.

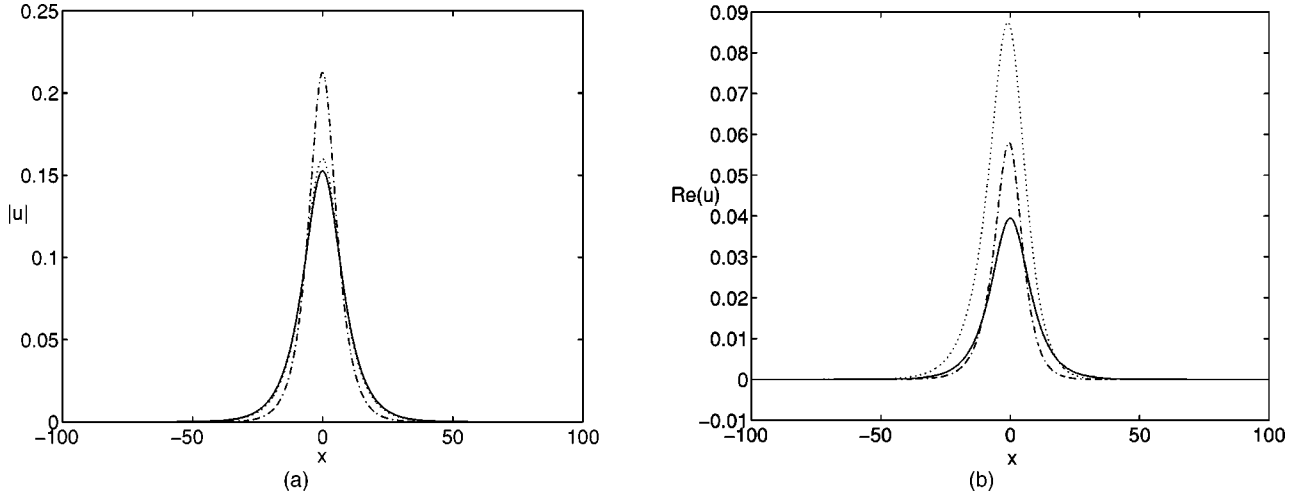

FIG. 4. The adiabatically approximated soliton solutions parametrized by the time evolution of the ODEs (24)–(26) at $t=0$ ($\cdots$), 25 (-··-), 1500 (—) (a) envelope (b) real part. Note that the graph for the soliton corresponding to the fixed point is the same as the solution at $t=1500$.

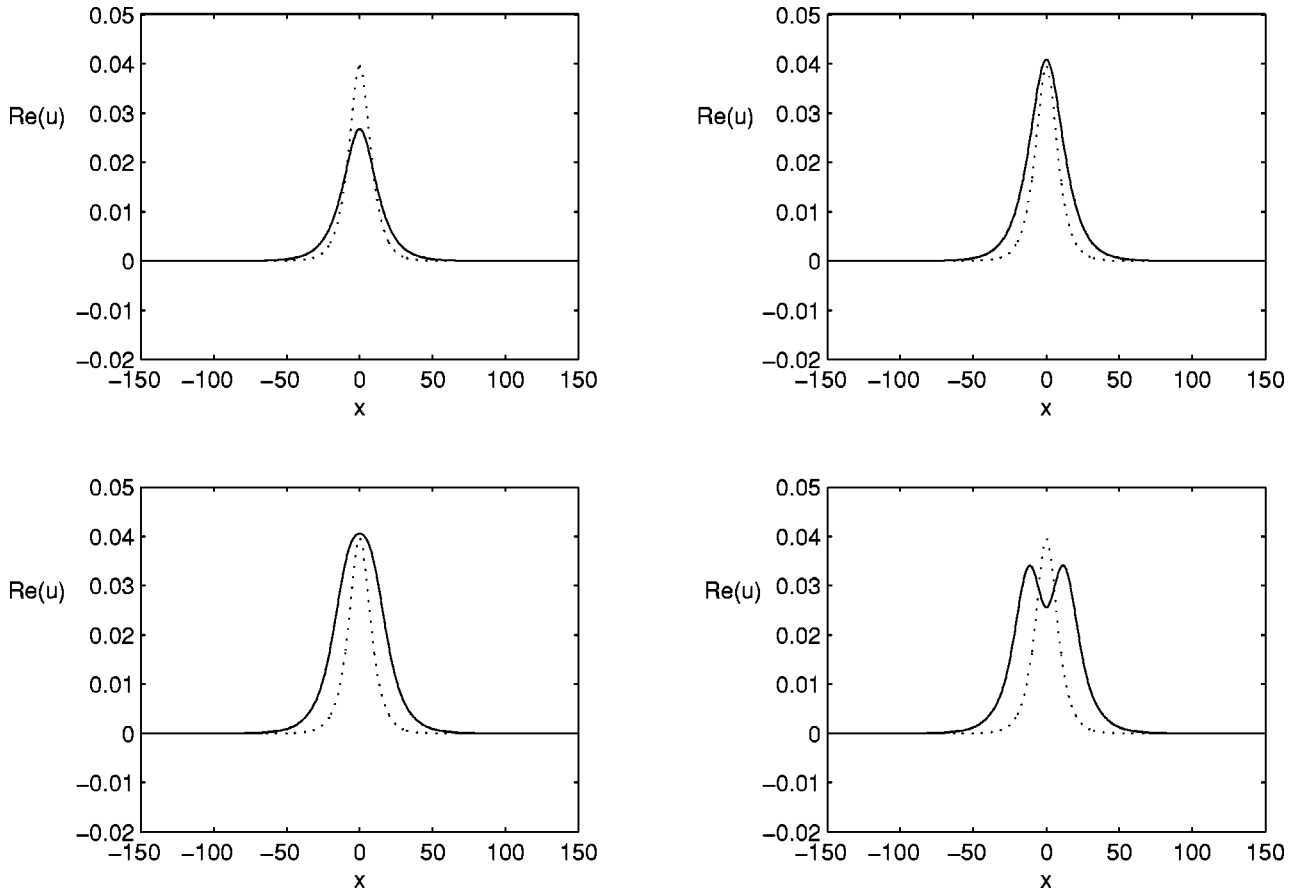

FIG. 5. Soliton solution (real part) corresponding to the nontrivial stable fixed point $(\cdots)$ and numerical solution of the perturbed nonlinear Schrödinger equation (—). Shown are real parts of the soliton at $t=0,30,80,120$ with initial condition of $u(x,0)=0.1\ \mathrm{sech}(0.1x)\exp(1.3i)$.

B. Perturbed nonlinear Schrödinger equation

1. Region a

For the simulations of the perturbed nonlinear Schrödinger equation, we present results for parameters $f=0.05$, $\delta=0.01$, and $\gamma=0.0125$. These values correspond to region *a* in Fig. 2. Other parameter values in region *a* show qualitatively similar features. Figure 5 shows that, given initial conditions near or a little away from the corresponding nonlinear fixed point, the real parts of the numerical solutions initially move to or stay near the adiabatic approximation of the nontrivial fixed point and then they lose their ''sech'' profiles. Tip splitting of the peak of the soliton destroys the shape of a one-soliton solution.

As time increases, the numerical solution continues to split the tip of the central peak until it develops regularly spaced patterns. Figure 6(a) shows patterns for four different initial conditions at $t=500$.

The tendency to approach the corresponding nontrivial fixed point solution can be seen in Fig. 7(b), which shows the distances (2-norm) between numerical solutions and the adiabatic stable soliton solution. The norm decreases initially for all initial conditions, but starts to increase eventually. It shows that the adiabatic soliton is unstable in the perturbed nonlinear Schrödinger equation, even though it is stable within the lower-dimensional approximation.

2. Region b

The parameters $f=0.05$, $\delta=-1.0$, and $\gamma=0.0125$ are representative for simulations in region *b* of Fig. 2. In this case, an initial condition near the stable fixed point leads to a stable soliton solution of the perturbed NLS. An initial condition corresponding to the snapshot of a moving soliton is shown in Fig. 8. The soliton initially moves to the right, but slows down and stops moving in a shape corresponding to the fixed point of the adiabatic approximation. The phase shift shows the effect of a variable ξ, describing the phase of the solitons, in Eqs. (19)–(22). In this parameter region, the adiabatic solution is stable not only for the lower-dimensional ordinary differential equation but also for the perturbed nonlinear Schrödinger equation.

C. Mathieu partial differential equation

It is important to note that an $O(1)$ time scale in the perturbed NLS [Eq. (5)] corresponds to an $O(1/\epsilon)$ time scale in averaged Mathieu PDE [Eq. (3)]. Hence, we expect the unstable soliton in region *a* to persist as an oscillon for a longer time.

For $\delta=0.01$, $f=0.05$, and $\gamma=0.0125$ (in the region of *a* in Fig. 2), Fig. 9 shows four snapshots within one period of an oscillon solution. The time evolution of such an oscillon is shown in Fig. 10. The solution oscillates and tends to

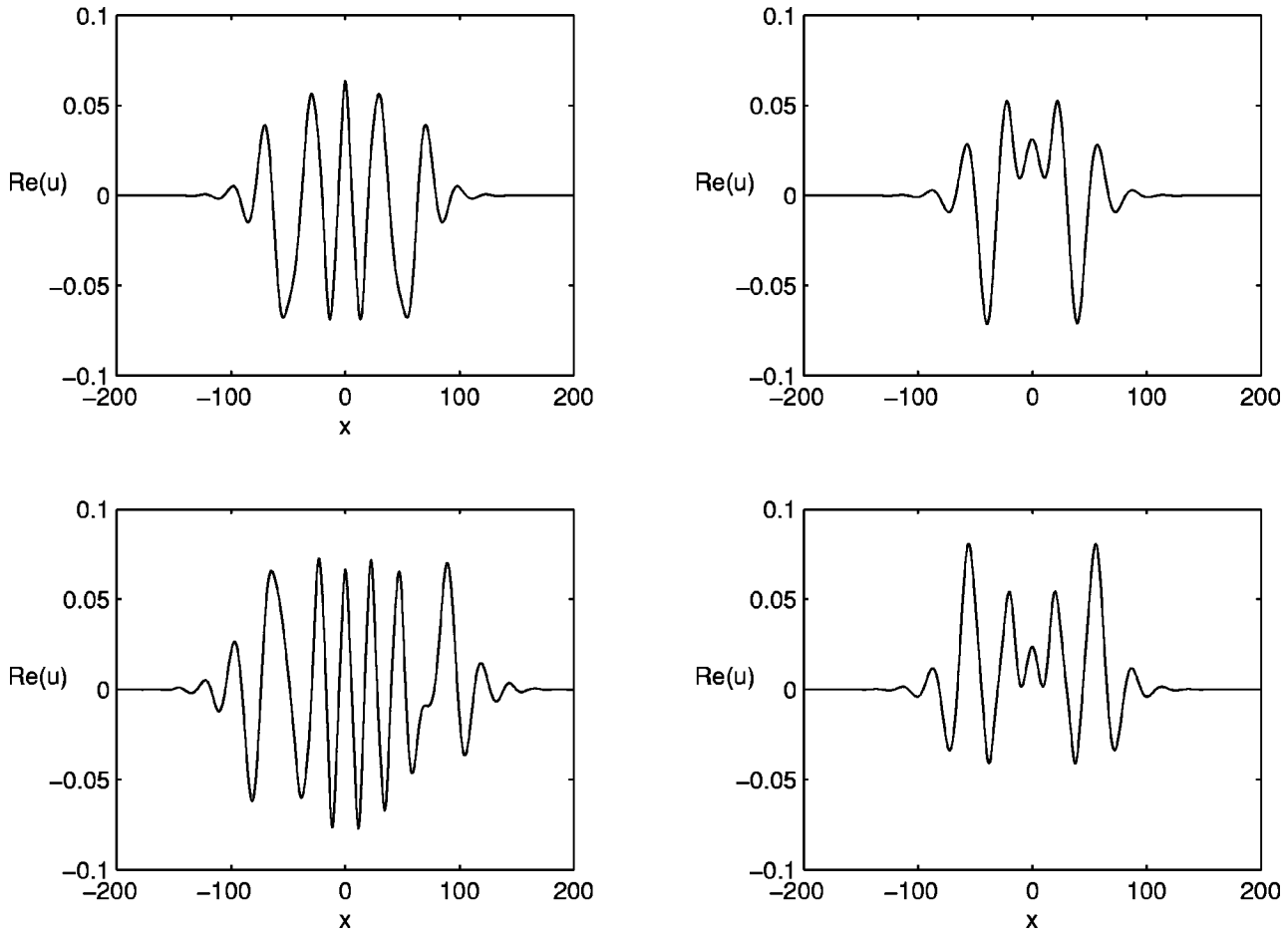

FIG. 6. Long time behavior of the real parts of the solutions of the perturbed NLS with various initial conditions at $t=500$: $u(x,0)=0.2\ \mathrm{sech}(0.2x)\exp(1.3i)$, $u(x,0)=0.15\ \mathrm{sech}(0.15x)\exp(0.0001x+1.2i)$, $u(x,0)=0.15\ \mathrm{sech}(0.15x)\exp(0.3x+1.3i)$, and $u(x,0)=0.15\ \mathrm{sech}(0.15x)\exp(0.3i)$.

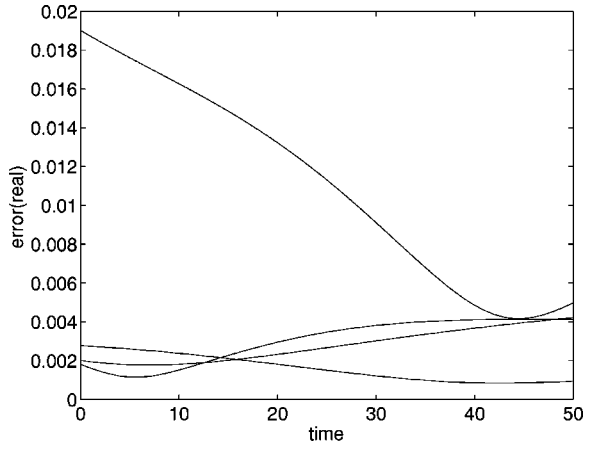

FIG. 7. Distances (2-norm) between the numerical solutions and the stable adiabatic soliton solution (real parts) with various initial conditions: $u(x,0)=0.2\ \mathrm{sech}(0.2x)\exp(1.3i)$, $u(x,0)=0.1\ \mathrm{sech}(0.1x)\exp(1.3i)$, $u(x,0)=0.15\ \mathrm{sech}(0.15x)\exp(0.0001x+1.2i)$, and $u(x,0)=0.15\ \mathrm{sech}(0.15x)\exp(0.3i)$.

adjust its amplitude to an oscillon initially. It loses its sech profile after a significantly longer time than in the case of the NLS.

In region of b of Fig. 2 (parameters $\delta=-0.7$, $f=0.1$, $\gamma=0.04$, $\epsilon=0.5$, $d=0.5$, and $\alpha=-4/3$), we find a oscillon-like solution (Fig. 11) that is stable for as long as we care to simulate. Typically, amplitude and profile of the oscillon are determined by the system parameters, regardless of initial condition. However, the final position of the oscillon is determined by the initial condition which may lead to a transient drift.

We also observe that solutions die out for different initial conditions. This corresponds to the fact that region b is a bistable region for the Mathieu PDE.

IV. CONCLUSION AND FUTURE WORK

We have studied the effect of parameteric driving on the formation of localized subharmonically oscillating patterns. Such patterns have been observed experimentally in shaking sand experiments and are called oscillons. As a prototype of such a parameterically driven pattern formation, we studied the Mathieu partial differential equation with weak damping, detuning, and nonlinearity. We showed that, upon averaging

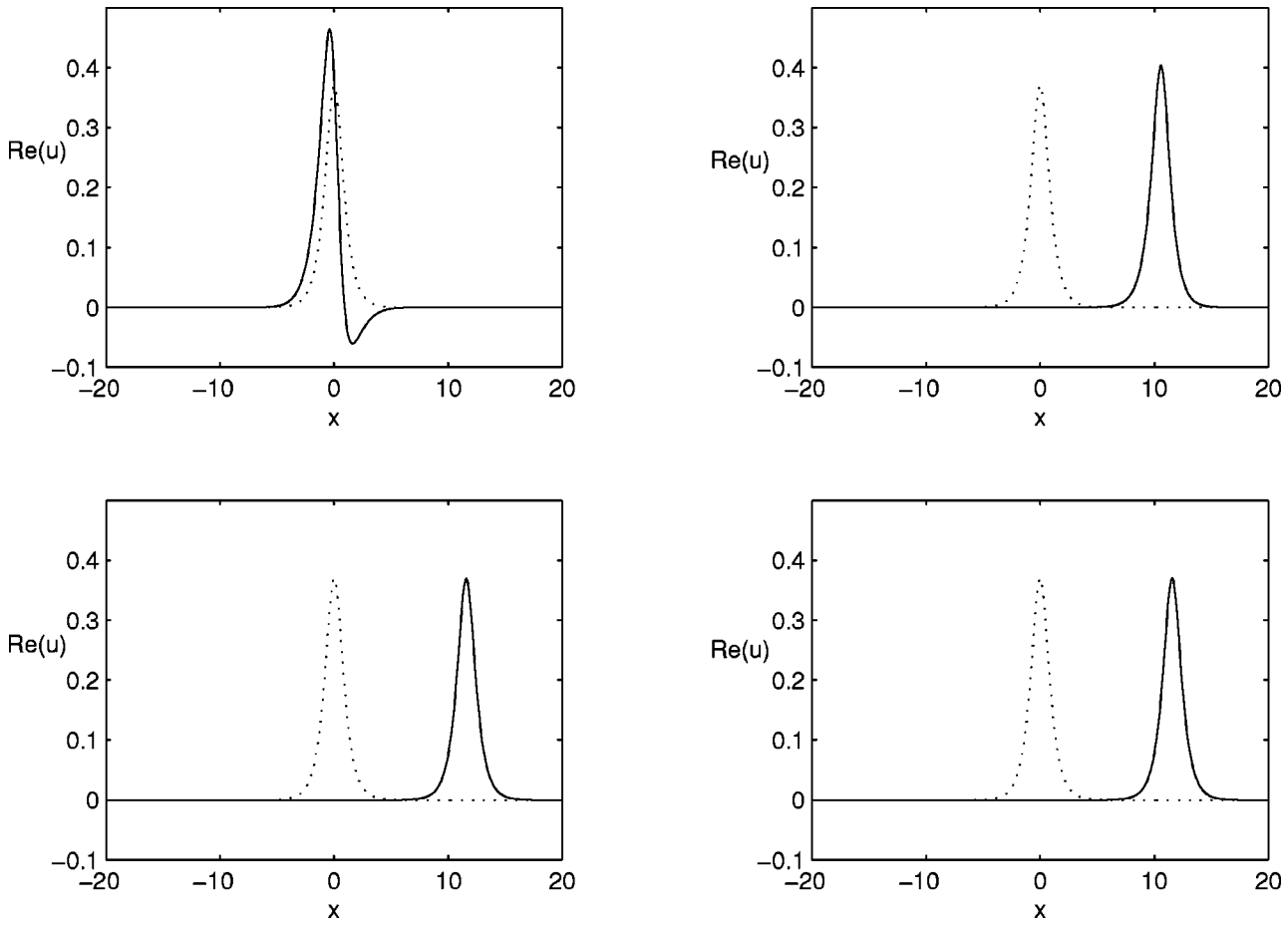

FIG. 8. The real part of the numerical solution (—) and the stable adiabatic solution ($\cdots$) at $t=0,100,400,$ and 800 with initial condition $u(x,0)=1.42\ \mathrm{sech}(1.42x)\exp(0.3x+1.3i)$.

the Mathieu PDE, the resulting system can be rescaled as a perturbed cubic nonlinear Schrödinger equation.

Adapting a perturbation method for solitons derived by Ref. [24], called the adiabatic approximation, we derive a system of ordinary differential equations which represents the time evolution of crucial parameters of a soliton (amplitude, frequency, and phase) under the perturbation terms coming from the Mathieu PDE. We show that nontrivial stable fixed points of this system of ODEs exist in the same parameter regions where the Mathieu equation has nontrivial fixed points. However, the fixed points of the adiabatic approximation represent isolated soliton solutions to the NLS equation which survive the presence of dissipative and forcing terms. This is reminiscent of a Melnikov analysis of a perturbation to an integrable nonlinear ODE [2], which allows us to determine the periodic orbit that survives the nonintegrable perturbations.

The resulting localized solution of the Mathieu PDE has many features of the oscillons: They are subharmonic, they do not drift (although most of the solitons of the NLS do), and they can be arbitrarily shifted in space, assuming an infinitely extended domain. Experimental evidence [7] shows similar features for the oscillons: They are localized, subharmonic, seem to occur at random positions, do not travel systematically but seem to jitter randomly.

The stability analysis of these localized solutions shows some interesting complications. Figure 2 shows two regions in the parameter space of forcing and detuning, labeled *a* and *b*, where we find stable solutions to the adiabatic ODE. Numerical simulations of the Mathieu PDE as well as the perturbed NLS, however, show stable attraction to the corresponding soliton solution of the Mathieu PDE only in region *b*. In region *a*, the simulations show an initial attraction to the steady soliton solution. However, after what seems like a time scale of $O(1)$ for the NLS and a time scale of $O(1/\epsilon)$ for the Mathieu PDE, the soliton shows successive tip splitting, until an extended pattern in space is achieved. In region *b*, depending on initial conditions, we also find solutions that become attracted to zero. Hence, region B is bistable for the Mathieu ODE and shows a stable localized oscillon solution for the Mathieu PDE. This corresponds to the fact that oscillons experimentally are associated with hysteresis.

Our analysis of the perturbed NLS is closely related to, and complements, earlier work by Laedtke and Spatschek [22] and by Elphick and Meron [23] on Faraday resonance in fluids. Laedke and Spatschek analyzed the homoclinic orbit (steady soliton) associated with the steady states of the perturbed NLS. They determined the stability of this stationary soliton by a linear perturbation analysis using operator theory of periodic Schrödinger operators. They found that

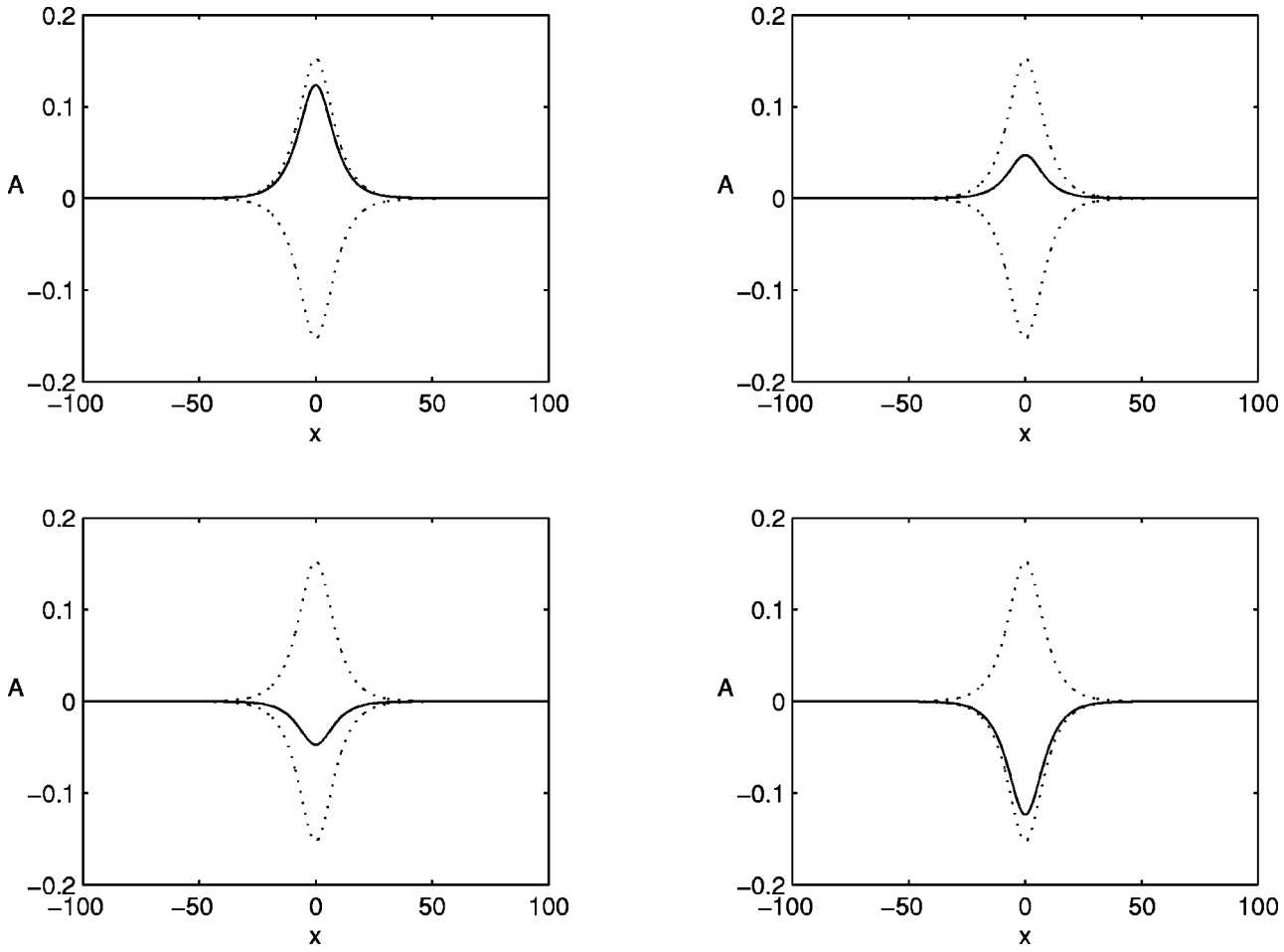

FIG. 9. Four snapshots within one period of the Mathieu PDE for $\delta=0.01$, $f=0.05$, $\gamma=0.01$ $\epsilon=0.01$, $d=0.5$, and $\alpha=-4/3$. The envelope corresponding to the fixed point of the ODEs is shown as the dashed line.

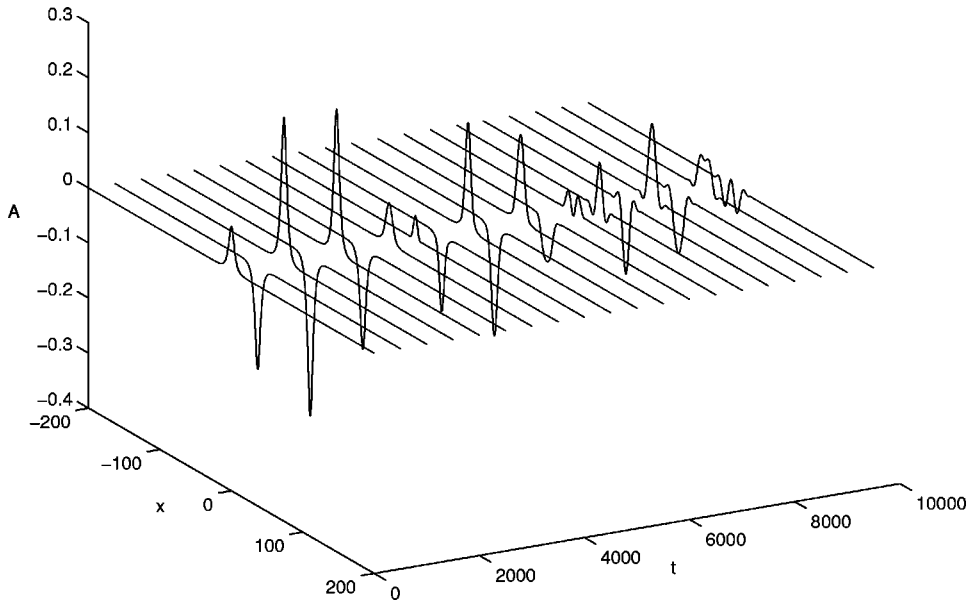

FIG. 10. Time evolution of the oscillonlike solution in the Mathieu PDE for an initial condition $A(x,0)=0.3\ \mathrm{sech}(0.3x)\cos(1.3)$, $A_t(x,0)=0.3\ \mathrm{sech}(0.3x)\sin(1.3)$. Parameters as in Fig. 9.

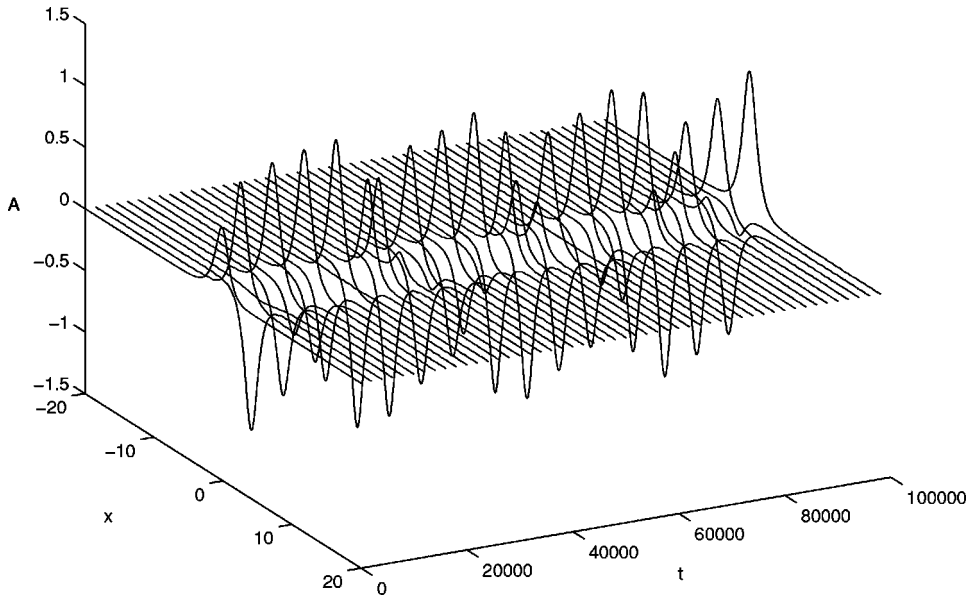

FIG. 11. Time evolution of a stable oscillonlike solution in the Mathieu PDE. Initial condition $A(x,0)=1.2\ \mathrm{sech}(1.2x)\cos(0.1x+1.1)$, $A_t(x,0)=1.2\ \mathrm{sech}(1.2x)\sin(0.1x+1.1)$.

the stationary solution is linearly unstable in region *a* in Fig. 2 and showed linear stability in region *b* for a restricted set of perturbations. Specifically, they show linear stability of the nontrivial soliton with phase shift zero with respect to odd-function perturbations. Numerical simulations confirmed the result and the transition to a regular pattern in region *a*.

Their work complements the research presented here in the following sense. The adiabatic approximation used here is a perturbation method on the *solution manifold of all* the soliton solutions of the NLS. Our analysis allows us to determine the dynamics on this solution manifold under perturbations. In this sense, it is a *global* method as opposed to local analysis. In particular, we show that in region *b*, the system has three surviving solutions; a stable soliton, an unstable soliton, and the stable trivial solution. A basin of attraction for the stable soliton can be estimated. The correct phase of the resulting stable localized solution can be determined based on an initial perturbation. Nevertheless, the adiabatic perturbation theory is still a finite-dimensional approximation to a PDE. In particular, it allows only perturbations that have zero boundary conditions at infinity. Hence, apparently, it does not include the perturbations, which makes the trivial solution unstable. This explains why Laedke and Spatschek found the correct stability of the localized solution in region *a* and why the adiabatic perturbation method misses it.

Elphick and Meron [23] derive the perturbed NLS [Eq. (7)] for the specific example of Faraday surface waves. They derive a system of differential equations closely related to our Eqs. (19)–(22) through an adiabatic-type perturbation method. Their analysis differs in two crucial points.

(1) The detuning term in Ref. [23] [δ in our Eq. (8)] is of one order larger than the forcing and the damping terms.

(2) The perturbed soliton has no slow time evolution of the phase.

As a result, in their ODEs for the perturbation equation the terms of the order of ϵ in equation for η and ω disappear. Hence, the fixed points corresponding to solitons that survive the perturbations are given by the solution of $\sin 2\tilde{\omega}=2\gamma/f$. Our analysis, which allows for a phase variation, adds a second constraint $\delta+2\nu^2+(f/2)\cos 2\tilde{\omega}=0$. Consequently, Elphick and Meron describe only the bifurcation near $f=2\gamma$ and $\delta<0$, i.e., the transition into region *b* in Fig. 2 from below.

Our study extends these results by setting all parameters δ,γ, and f to the same order of magnitude. In effect this treats the problem as a degenerate bifurcation problem, which allows an unfolding in a ball around $(\delta,\gamma,f)=(0,0,0)$, thus allowing to extend the analysis to $\delta>0$ as well as to the region *a* of Fig. 2. Additionally, by allowing for a slow time dependence of the phase, we can use the time evolution of ξ [Eq. (21)] to determine the eventual exact position of the soliton where it stops traveling, as a function of its initial perturbation.

There are the following interesting avenues for future work.

(1) We studied the cubic nonlinearity in the Mathieu PDE that leads to the focusing nonlinear Schrödinger equation. In

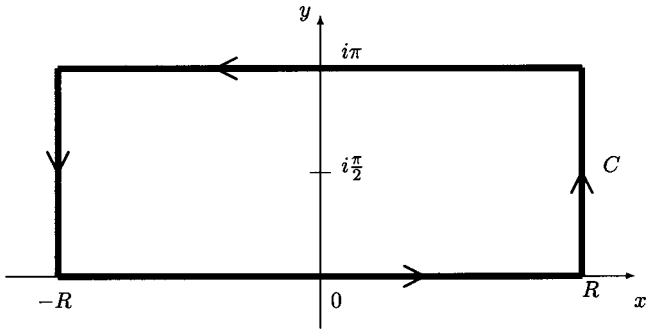

FIG. 12. Integration contour *C*.

a subsequent work, we will extend the work of Ref. [23] who have also studied the defocusing case corresponding to a dark soliton for the NLS to include a ball around $(\delta,\gamma,f)=(0,0,0)$ in parameter space.

(2) Experiments are done with a two-dimensional surface, and oscillons are really rotationally symmetric objects. The extension of the Mathieu PDE to two spatial dimensions replaces the second-order spatial derivative by a Laplacian. However, the resulting averaged equation is not a simple perturbation of the NLS and cannot be studied directly via the same perturbation methods. It remains to be seen whether symmetry will allow us to reduce the two-dimensional system to the present study.

(3) Experiments are done in a finite domain. It seems reasonable to expect that approximate solitons will survive in a finite domain that is an order of magnitude larger than a characteristic length of the soliton, but that needs to be proven. We would also expect that there is a boundary region of the size of the characteristic length of the soliton where boundary conditions and the soliton interact to form new dynamics.

(4) Experiments show interacting oscillons: there are two and three oscillon molecules [7] as well as almost spatially extended oscillon patterns. A first step to model these interacting oscillons is to study the perturbation theory of interacting solitons.

ACKNOWLEDGMENTS

This research was supported by NSF Grant No. DMS-0204543. We thank Bjorn Birnir who made us aware of Ref. [22].

APPENDIX: EVALUATION OF EQS. (11)–(14)

The integrals in the Eqs. (11)–(14) can be evaluated by a complex integration using the residue theorem. Let $z=x+iy$ be a complex variable and $f(z)$ be a complex valued function such that

$$f(z)=\tanh z\,\mathrm{sech}^2 z e^{isz} \tag{A1}$$

for any real value s. Then, $f(z)$ has singularities at $z=i(k+1/2)\pi$ for integers k. Let C be the contour as shown in Fig. 12 consisting of the real axis from $-R$ to R, $z=i\pi, -R\leqslant x\leqslant R$ and two lines parallel to the y axis, $z=R$, $0\leqslant y\leqslant\pi$ and $z=-R$, $0\leqslant y\leqslant\pi$.

Then, the only singularity of $f(z)$ inside C is at $z=i\pi/2$, say z_0. Since $f(z)$ has a pole of the order of 3 at $z=z_0$, the residue can be calculated as

$$\text{residue}=\frac{1}{2!}\lim_{z\to z_0}\frac{d^2}{dz^2}(z-z_0)^3 f(z)=\frac{1}{2}s^2 e^{-\pi s/2}. \tag{A2}$$

It is clear that the index of C with respect to z_0 is 1 since contour C rotates around z_0 once counterclockwise.

Theorem 1 (Residue Theorem). Let A be a region and $z_1,\ldots,z_n\in A$ be n distinct points in A. Let f be analytic on A except for isolated singularities at $z_1,z_2,\ldots,z_n$. Let C be a closed curve in A homotopic to a point in A. Assume that no z_i lies on C. Then,

$$\int_C f(z)dz=2\pi i\sum_{i=1}^{n} res(f,z_i)ind(C,z_i), \tag{A3}$$

where $res(f,z_i)$ is the residue of f at z_i and $ind(C,z_i)$ is the index of C with respect to z_i [33].

After applying the residue theorem, we have

$$\int_C \tanh z\,\mathrm{sech}^2 z e^{isz}dz=i\pi s^2 e^{-\pi s/2}. \tag{A4}$$

On the other hand,

$$\begin{aligned}\int_C \tanh z\,\mathrm{sech}^2 z e^{isz}dz &= \int_{-R}^{R}\tanh x\,\mathrm{sech}^2 x e^{isx}dx+\int_0^{\pi}\tanh(R+iy)\mathrm{sech}^2\\ &\times(R+iy)e^{is(R+iy)}dy+\int_R^{-R}\tanh(x+i\pi)\\ &\times\mathrm{sech}^2(x+i\pi)e^{is(x+i\pi)}dx+\int_{\pi}^{0}\tanh(-R+iy)\\ &\times\mathrm{sech}^2(-R+iy)e^{is(-R+iy)}dy.\end{aligned} \tag{A5}$$

Observe that

$$\lim_{R\to\infty}\int_0^{\pi}\tanh(R+iy)\mathrm{sech}^2(R+iy)e^{is(R+iy)}dy=0, \tag{A6}$$

$$\lim_{R\to\infty}\int_{\pi}^{0}\tanh(-R+iy)\mathrm{sech}^2(-R+iy)e^{is(-R+iy)}dy=0, \tag{A7}$$

and

$$\begin{aligned}\int_R^{-R}\tanh(x+i\pi)\mathrm{sech}^2(x+i\pi)e^{is(x+i\pi)}dx &= -e^{-\pi s}\int_{-R}^{R}\tanh x\,\mathrm{sech}^2 x e^{isx}dx.\end{aligned} \tag{A8}$$

Therefore,

$$\begin{aligned}\lim_{R\to\infty}\int_C \tanh z\,\mathrm{sech}^2 z e^{isz}dz &= (1-e^{-\pi s})\int_{-\infty}^{\infty}\tanh x\,\mathrm{sech}^2 x e^{isx}dx,\end{aligned} \tag{A9}$$

and

$$\int_{-\infty}^{\infty}\tanh x\,\mathrm{sech}^2 x e^{isx}dx=i\frac{\pi s^2 e^{-\pi s/2}}{1-e^{-\pi s}}=i\frac{\pi s^2}{2}\mathrm{csch}\left(\frac{\pi s}{2}\right) \tag{A10}$$

from Eq. (A4). Similarly, one can find

$$\int_{-\infty}^{\infty} \operatorname{sech}^2 x e^{isx} dx = \pi s \operatorname{csch}\left(\frac{\pi s}{2}\right), \tag{A11}$$

$$\int_{-\infty}^{\infty} x \operatorname{sech}^2 x e^{isx} dx = i\pi \operatorname{csch}\left(\frac{\pi s}{2}\right)\left[\frac{\pi s}{2}\coth\left(\frac{\pi s}{2}\right) - 1\right], \tag{A12}$$

$$\int_{-\infty}^{\infty} x \tanh x \operatorname{sech}^2 x e^{isx} dx = \pi s \operatorname{csch}\left(\frac{\pi s}{2}\right)\left[1 - \frac{\pi s}{4}\coth\left(\frac{\pi s}{2}\right)\right], \tag{A13}$$

for any real s.

[1] V. Arnold, *Mathematical Methods of Classical Mechanics* (Springer-Verlag, Berlin, 1978).
[2] J. Guckenheimer and P. Holmes, *Nonlinear Oscillations, Dynamical Systems, and Bifurcations of Vector Fields* (Springer-Verlag, Berlin, 1983).
[3] R. Rand, W. Newman, B.C. Denardo, and A. Newman, in *Proceedings for the 1995 Design Engineering Technical Conference* (ASME, Boston, 1995), Vol. 3, Part A, pp. 57–68.
[4] W. Newman, R. Rand, B.C. Denardo, and A. Newman, Chaos **9**, 242 (1999).
[5] D. Armbruster, M. George, and I. Oprea, Chaos **11**, 52 (2001).
[6] A. Kudrolli and J. Gollub, Physica D **97**, 133 (1996).
[7] P. Umbanhowar, F. Melo, and H.L. Swinney, Nature (London) **382**, 793 (1996).
[8] J. Wu, R. Keolian, and I. Rudnick, Phys. Rev. Lett. **52**, 1421 (1984).
[9] J. Bruyn, C. Bizon, M. Shattuck, D. Goldman, J. Swift, and H. Swinney, Phys. Rev. Lett. **81**, 1421 (1998).
[10] Y. Kivshar and B. Malomed, Rev. Mod. Phys. **61**, 763 (1989).
[11] Y. Kivshar and D. Pelinovsky, Phys. Rep. **331**, 117 (2000).
[12] V. Hakim and Y. Pomeau, Eur. J. Mech. B/Fluids, Suppl. **10**(2), 137 (1991).
[13] W. Saarloos and P. Hohenberg, Physica D **56**, 303 (1992).
[14] P. Coullet, J. Lega, B. Houchmanzadeh, and J. Lajzerowicz, Phys. Rev. Lett. **65**, 1352 (1990).
[15] P. Coullet and K. Emilsson, Physica D **61**, 119 (2002).
[16] C. Elphick, A. Hagberg, B.A. Malomed, and E. Meron, Phys. Lett. A **230**, 33 (1997).
[17] C. Elphick, A. Hagberg, and E. Meron, Phys. Rev. Lett. **80**, 5007 (1998).
[18] C. Crawford and H. Riecke, Physica D **129**, 83 (1999).
[19] Y. Pomeau, Physica D **23**, 3 (1986).
[20] E. Meron, Phys. Rep. **218**, 1 (1992).
[21] J. Miles, J. Fluid Mech. **146**, 285 (1984).
[22] E. Laedke and K. Spatschek, J. Fluid Mech. **223**, 589 (1991).
[23] C. Elphick and E. Meron, Phys. Rev. A **40**, 3226 (1989).
[24] V. Karpman and E. Maslov, Sov. Phys. JETP **46**, 281 (1977).
[25] A. Nayfeh and D. Mook, *Nonlinear Oscillations* (Wiley, New York, 1979).
[26] J. Sanders and F. Verhulst, *Averaging Methods in Nonlinear Dynamical Systems* (Springer-Verlag, Berlin, 1985).
[27] J. Norris, Int. J. Bifurcation Chaos Appl. Sci. Eng. **4**, 71 (1994).
[28] K. Nozaski and N. Bekki, Physica D **21**, 381 (1986).
[29] D. McLaughlin, E. Overman, S. Wiggins, and C. Xiong, *Dynamics Reported: Expositions in Dynamical Systems* (New Series) (Springer-Verlag, Berlin, 1996), p. 190.
[30] B. Birnir and R. Grauer, Commun. Math. Phys. **162**, 539 (1994).
[31] A. Hasegawa and Y. Kodama, *Solitons in Optical Communications* (Oxford University, New York, 1995).
[32] D. Kaup, SIAM (Soc. Ind. Appl. Math.) J. Appl. Math. **31**, 121 (1976).
[33] J. Marsden, *Basic Complex Analysis* (Freeman, San Fransisco, 1973).